Impact of radiative cooling on the thermal behavior of multi-junction solar cells

Impact of radiative cooling on the thermal behavior of multi-junction solar cells

Pietro Testa*[a], Gemma Giliberti[a], Matteo Cagnoni[a], Federica Cappelluti[a]
[a] Department of Electronics and Telecommunications, Politecnico di Torino, C.so degli Abruzzi 24, 10129 Turin, Italy

Abstract

Thermal radiation is a key aspect of solar cell thermal management. In this work we study, through detailed balance and multiphysics simulations, the thermal behavior of multi-junction solar cells and the impact of different radiative cooling designs on their achievable efficiency. We discuss the influence of the mid-infrared emissivity of the semiconductors constituting the cell and possible encapsulating materials, with the goal of evaluating the performance improvements achievable with an ideal thermal emitter.

Keywords: Radiative cooling, multi-junction solar cells, detailed-balance model, thermal management, multiphysics model.

1. INTRODUCTION

High operating temperature results in performance degradation and reduced lifespan of solar cells [1]. Even cutting-edge technologies such as multi-junction solar cells, despite the mitigation of thermalization and sub-band gap losses, experience significant self-heating, demanding for effective thermal management strategies, especially in concentrating photovoltaics systems [2]. Radiative cooling, i.e., the dissipation of heat through the emission of infrared radiation via the atmospheric transparency window (8–13 μm) [3], is a cost-effective and easily integrable passive approach routinely applied in photovoltaic modules, by means mainly of the front cover glass and encapsulating materials [4]. In recent years, a substantial literature has emerged aimed at developing novel and optimized radiative cooling materials and designs [5], [6], [7], [8], [9] and assessing their effectiveness on solar cell performance.

In [10] we presented a detailed balance model to analyze the impact of ideal radiative cooling on the steady-state temperature and efficiency of multi-junction solar cells, under unconcentrated and low-concentrated light. In this work, we extend that study by modeling the radiative cooler with literature-based thermal emissivity spectra of various photovoltaic cells, both bare and encapsulated, to quantify more accurately the gain that can be expected by optimized radiative cooling with respect to today's technology. While most reported emissivity data are measured at normal incidence, thermal radiation effectiveness is significantly affected by the emissivity value at high angles [4], [11]. Hence, we generalize the analysis based on a simple parametrized model of the angular and amplitude dependence of emissivity. Finally, we present preliminary results of a multiphysics simulation of a triple-junction solar cell integrated into a photovoltaic module. The simulation combines electromagnetic calculations, based on the scattering matrix method for incoherent layers, with a thermal model of the photovoltaic module. By incorporating angular emissivity data and accounting for heat diffusion within the module, this study provides a comprehensive analysis of radiative cooling effectiveness in a practical scenario.

2. METHODS

Figure 1 illustrates the structure and main power terms of the detailed-balance model and multiphysics models used to evaluate radiative cooling performance.

In the detailed balance model in Figure 1(a), the system consists of three components arranged vertically: a radiative cooler at the top, a solar cell in the middle, and a perfect, insulating mirror at the bottom. The temperature is assumed to be uniform throughout the system and is determined as the temperature corresponding to the thermal equilibrium condition, set by zero net power exchange between the system and the ambient:

$$P_{\text{net}} = P_{\text{rad}}^{\text{RC}} - P_{\text{atm}} + P_{\text{con}} + P_{\text{rad}}^{\text{SC}} + P_{\text{elec}} - P_{\text{sun}} = 0$$

where $P_{\text{rad}}^{\text{RC}}$ and P_{atm} are the power density radiated and absorbed from the atmosphere by the radiative cooler, respectively.

*pietro.testa@polito.it; federica.cappelluti@polito.it.

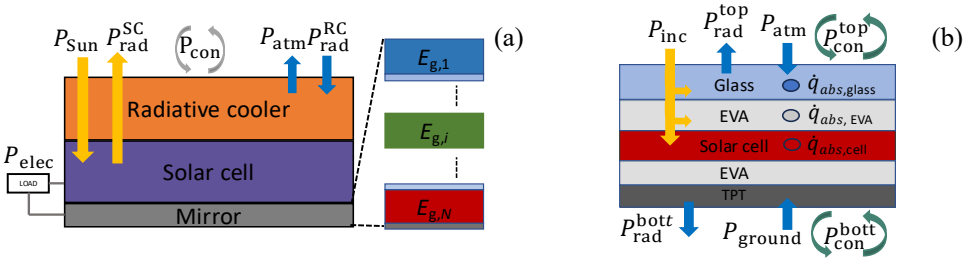

Figure 1. Energy flows involved in the detailed balance model describing a solar cell coupled with a radiative cooler (a) and in the electromagnetic-thermal model describing an encapsulated solar cell (b).

P_{con} represents the power exchanged with the surroundings by nonradiative heat transfer mechanisms, modeled as $P_{con} = h_c(T\text{-}T_0)$ with $h_c = 10.6$ W/m^2/K (average wind case) and T_0 the ambient temperature. P_{rad}^{SC}, P_{elec} and P_{sun} are the power radiated, delivered to the load, and absorbed from the Sun by the solar cell. They are calculated according to the Shockley-Queisser model of series connected multijunction cells, whose assumptions and details are provided in [9]. In this modeling approach the solar cell and radiative cooler are spectrally separated, but since they are isothermals, the thermal emissivity associated to the radiative cooler can model the inherent emissivity of the solar cell. The detailed balance analysis considers different solar cell technologies. Assumed bandgaps are: 1.12 eV for c-Si, 1.1 eV for CIGS, 1.55 eV for CdTe, and 1.87/1.4/0.67 eV for the triple junction Ge/GaAs/InGaP.

The multiphysics model in Figure 1(b) considers a standard assembly of a solar cell, consisting of cover glass, two EVA encapsulant layers, and Tedlar (TPT) back sheet, all having the same area. Heat diffusion and temperature distribution through the module are simulated using finite element modeling in COMSOL Multiphysics. The solar power absorbed by each layer is modeled as a heat source, considering the materials optical coefficients in Table 1, which represent the percentage of absorbed, transmitted, and reflected sun power [12]. The power absorbed by the solar cell is weighted by $\big(1-\eta(T)\big)$, which accounts for the fraction of solar power not converted into electricity. The temperature-dependent efficiency is modeled as $\eta(T) = \eta_{ref}\,[1-\beta\cdot(T-T_{ref})]$, being η_{ref} and T_{ref} the efficiency and temperature in standard operating conditions and β the efficiency temperature coefficient. The solar cell thermal conductivity was approximated with that of the Ge bulk layer. Radiative heat transfer between the structure and its surroundings (sky and ground) is modeled as boundary heat fluxes in COMSOL. These fluxes are calculated externally in MATLAB using a scattering matrix method for coherent and incoherent propagation to model the angle- and wavelength-dependent emissivity, as COMSOL does not natively support this feature. In the following example, radiated and absorbed power at the front surface were calculated from the spectral and angular emissivity primarily defined by the glass. For the rear surface, a constant emissivity of 0.9 was assumed for the TPT layer. Table 1 summarizes the material parameters and dimensions of each layer used in the simulations. Nonradiative heat transfer at the top and rear surface is calculated following the approach outlined in the detailed balance model.

Table 1 Layers dimension and materials parameters used in the simulations.

	d (mm)	κ (W/ m K)	c_p (J/ kg K)	ρ (kg/m^3)	a	r	t
Glass	2	2.00	500	2450	0.04	0.04	0.92
EVA	0.5	0.31	2090	950	0.08	0.02	0.90
Ge	0.15	60	310	5320	0.92	0.08	-
TPT	0.3	0.15	125	1200	-	-	-

3. RESULTS

As first, we compare in Figure 2(a) the temperature and efficiency of solar cells with one, two, and three junctions, calculated according to the detailed balance model, as a function of the lowermost subcell band gap, in the limit cases of ideal radiative cooling (thermal emissivity = 1 for wavelengths > 4 μm) and no radiative cooling (zero thermal emissivity). As shown in Figure 2(a), the temperature reduction due to radiative cooling is more significant as the bandgap and number of junctions decrease. The correlated efficiency gain follows a similar trend, as shown in the inset. Looking at the colored

circles, which mark energy gap configurations with the highest efficiency for multi-junction cells and the silicon gap for the single-junction case, respectively, it turns out that the (absolute) increase in efficiency due to perfect radiative cooling is similar (about 1%) in all cells regardless of the more modest temperature reduction experienced by multi-junction cells compared to single-junction cells. This is because multi-junction solar cells have a higher efficiency temperature coefficient compared to single-junction solar cells [10].

However, using the zero infrared emissivity case as benchmark is overly simplistic for quantifying the actual gains achievable by optimizing radiative cooling in today's solar cells and modules. Therefore, we have collected experimental data of wavelength dependent thermal emissivity for a few representative photovoltaic technologies. Figure 2b shows examples of measured emissivity values, at normal incidence, for common bare and encapsulated solar cells reported in the literature for crystalline silicon cells [6], [13], CIGS [14], CdTe [15], and a triple junction Ge/GaAs/InGaP [9]. The emissivity of bare cells strongly depends on the materials and design of the device, whereas encapsulated cells generally exhibit similarly high emissivity in the mid- and far-infrared regions, primarily due to the cover glass and characterized by a pronounced dip around 9 μm wavelength. An exception is observed in CIGS solar cells, where a polysilazane layer, used as an encapsulant for flexible solar cells, significantly reduces emissivity [14]. By introducing these emissivity values into the detailed balance model, we calculated the absolute efficiency increase that bare and encapsulated solar cells can achieve due to the temperature reduction provided by radiative cooling. The results are compared to the perfect emitter case in Figure 2c, where the steady-state temperature for each case study is also reported. All encapsulated cells perform very well, with a temperature difference compared to the ideal emitter of about 1.5 K for all case studies except for the CIGS one where it increases to about 4 K. The corresponding room for improvement in terms of absolute efficiency, assuming ideal cells operating in the radiative limit, is on the order of about 0.1%-0.2 %, and plausibly a bit larger when considering non radiative recombination mechanisms [16]. Bare cells are obviously less performing, denoting the importance of designing and optimizing encapsulating materials not only for structural integrity and protection but also for effective thermal radiation. Especially for solar cells encapsulated with materials other than glass, such as flexible solar cells using polyethylene [17] or other polymers [14], with low emissivity in the infrared region, the potential temperature reduction and efficiency gain from optimizing infrared emissivity are relevant.

With the goal of optimizing thermal emissivity, an aspect to consider is its angular dependence. The emissivity spectra

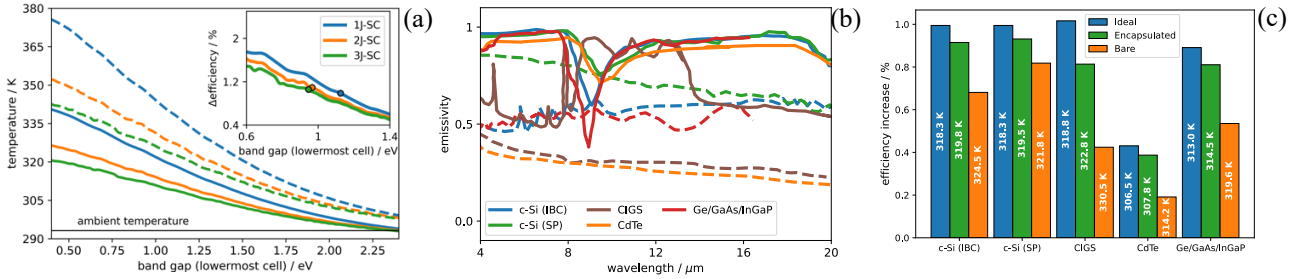

Figure 2. (a) Operating temperature and efficiency gain of MJSCs with *ideal thermal emissivity* (solid lines) and with *zero thermal emissivity* (dashed lines) as a function of the lowermost cell band gap. *Data from [10].* (b) *M*easured emissivity for different bare (dashed lines) and encapsulated solar cells (solid line) as *a* function of the wavelength for c-Si interdigitated-back-contact (IBC) [6], c-Si with screen-printed (SP) silver front and aluminum rear contacts [13], CIGS [14], CdTe [15], Ge/GaAs/InGaP [9]. (c) Comparison of steady-state temperature and absolute efficiency gain (with respect to the limit case of absent thermal radiation) for different technologies considering ideal emissivity and the experimental data in (b).

used in this study (Figure 2b) were measured at normal incidence, leading to slightly overestimating the cooling effect [4], [11]. As an example, Figure 3a shows the calculated angular dependence of the emissivity of soda-lime glass (3.2 mm thick). For angles greater than 70°, the emissivity drops significantly. A rough indication of the impact of this effect can be derived by considering a simple step-like model for the thermal emissivity profile, which is defined by two parameters: amplitude and cutoff angle (ϑ_{lim}). For $\vartheta \leq \vartheta_{\mathrm{lim}}$ the thermal emissivity is constant, while for $\vartheta > \vartheta_{\mathrm{lim}}$, it drops to zero. Figure 3b reports the achievable temperature reduction for the case of a three-junction solar cell as a function of the emissivity amplitude and cutoff angle. Results show a modest but non negligible dependence of the predicted temperature reduction on the cutoff angle. When the emissivity amplitude is high, by realizing it as more isotropic as possible, a few degrees of temperature reduction can be achieved.

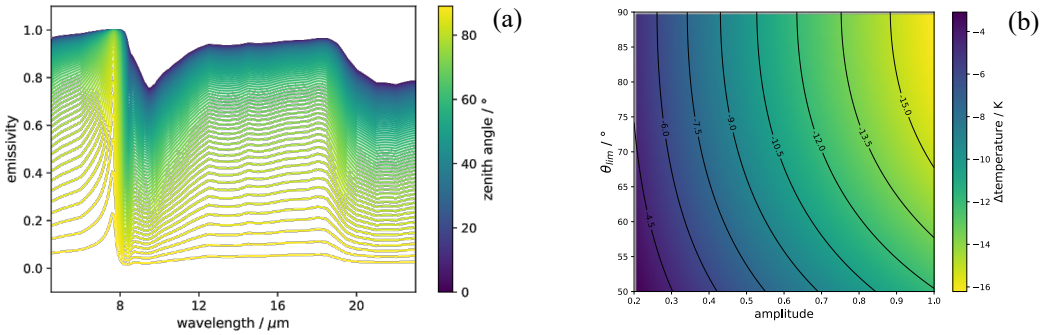

Figure 3. (a) Directional spectral emissivity soda lime glass. (b) Temperature reduction provided by an ideal cooler to a 3J solar cell as function of the amplitude and cutoff angle of the infrared emissivity.

Finally, we studied by coupled electromagnetic and thermal simulations a more realistic case, made by a triple junction cell (with efficiency of 25.2% and temperature coefficient of $-0.33\ \%/\mathrm{K}$ [18]) encapsulated in the module structure sketched in Figure 1b. Figure 4 presents the temperature profile across the device calculated from the multiphysics simulation. For a qualitative comparison with the previously analyzed case studies of ideal, bare cell, and encapsulated cell emissivity, the glass is simulated with the corresponding emissivity spectra: the ideal one, that one characteristic of the bare triple-junction cell in Fig. 2b, and the angle-dependent emissivity spectra reported in Figure 3a for soda lime glass. In all cases, the temperature is obviously higher than in the detailed balance model (Figure 3b) because of the lower cell efficiency. The temperature profile across the system is rather uniform, validating the hypothesis of almost isothermal conditions used in the detailed balance mode. Finally, the predicted temperature difference between the different cases is in line with the detailed balance model results, confirming that optimization of standard encapsulation methods can provide an improvement of less than 2 K. On the other hand, in the perspective of concentrated systems the advantage can become more significant, as shown by the higher rate of temperature increase with concentration shown in Figure 4(b). Furthermore, in single cell concentrating photovoltaic systems, it is straightforward to scale up the area of the glass or any other emitting surface relative to that of the cell., increasing the temperature reduction achievable by radiative cooling, provided that lateral thermal spreading is also efficient [10].

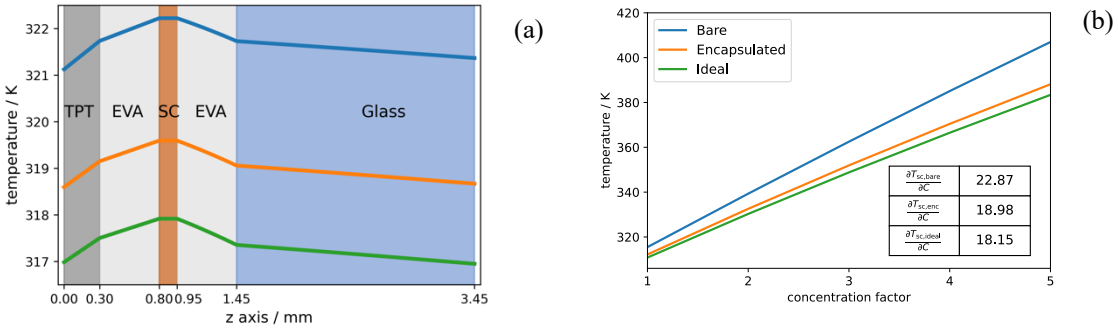

Figure 4 (a) Temperature profile within a PV module with bare (blue line), glass (orange line), and ideal emissivity (green line). (b) Solar cell temperature vs. concentration factor for different case studies of thermal emissivity.

4. CONCLUSION

In this study we have analyzed the effect of radiative cooling in the thermal management of solar cells, with a focus on multi-junction cells, by detailed balance and multiphysics modeling. Common solar cells show high variability in emissivity depending on the considered technology, but in general encapsulated solar cells already exhibit near-ideal

thermal radiation, primarily due to the high infrared emissivity of the cover glass. The reported results show that optimizing existing module materials and designs will allow limited temperature reduction, which, however, might turn into significant gains in terms of lifespan of the system and possibly on its energy yield. Under concentration and in space applications the advantage is more evident. As for emerging technologies, especially for flexible and lightweight solar cells, it is important to design encapsulating materials with high infrared emissivity, at least comparable to that one of standard photovoltaics.

ACKNOWLEDGEMENTS

This project has received funding from the European Union's Horizon 2020 Research and Innovation Program under grant agreement no. 964450.

REFERENCES

[1] O. Dupré, R. Vaillon, and M. A. Green, *Thermal Behavior of Photovoltaic Devices*. Cham: Springer International Publishing, 2017. doi: 10.1007/978-3-319-49457-9.

[2] A. Royne, C. J. Dey, and D. R. Mills, 'Cooling of photovoltaic cells under concentrated illumination: a critical review', *Solar Energy Materials and Solar Cells*, vol. 86, no. 4, pp. 451–483, Apr. 2005, doi: 10.1016/j.solmat.2004.09.003.

[3] A. P. Raman, M. A. Anoma, L. Zhu, E. Rephaeli, and S. Fan, 'Passive radiative cooling below ambient air temperature under direct sunlight', *Nature*, vol. 515, no. 7528, pp. 540–544, Nov. 2014, doi: 10.1038/nature13883.

[4] A. R. Gentle and G. B. Smith, 'Is enhanced radiative cooling of solar cell modules worth pursuing?', *Solar Energy Materials and Solar Cells*, vol. 150, pp. 39–42, Jun. 2016, doi: 10.1016/j.solmat.2016.01.039.

[5] B. Zhao, M. Hu, X. Ao, N. Chen, and G. Pei, 'Radiative cooling: A review of fundamentals, materials, applications, and prospects', *Applied Energy*, vol. 236, pp. 489–513, Feb. 2019, doi: 10.1016/j.apenergy.2018.12.018.

[6] W. Li, Y. Shi, K. Chen, L. Zhu, and S. Fan, 'A Comprehensive Photonic Approach for Solar Cell Cooling', *ACS Photonics*, vol. 4, no. 4, pp. 774–782, Apr. 2017, doi: 10.1021/acsphotonics.7b00089.

[7] Z. Zhou, Z. Wang, and P. Bermel, 'Radiative cooling for low-bandgap photovoltaics under concentrated sunlight', *Opt. Express, OE*, vol. 27, no. 8, pp. A404–A418, Apr. 2019, doi: 10.1364/OE.27.00A404.

[8] M. Cagnoni, A. Tibaldi, J. S. Dolado, and F. Cappelluti, 'Cementitious Materials as Promising Radiative Coolers for Solar Cells', *iScience*, p. 105320, Oct. 2022, doi: 10.1016/j.isci.2022.105320.

[9] S.-Y. Heo, D. H. Kim, Y. M. Song, and G. J. Lee, 'Determining the Effectiveness of Radiative Cooler-Integrated Solar Cells', *Advanced Energy Materials*, vol. 12, no. 10, p. 2103258, 2022, doi: 10.1002/aenm.202103258.

[10] P. Testa, M. Cagnoni, and F. Cappelluti, 'Detailed-balance assessment of radiative cooling for multi-junction solar cells under unconcentrated and low-concentrated light', *Solar Energy Materials and Solar Cells*, vol. 274, p. 112958, Aug. 2024, doi: 10.1016/j.solmat.2024.112958.

[11] I. G. De Arrieta, T. Echániz, R. Fuente, and G. A. López, 'Angle-Resolved Direct Emissivity Measurements on Unencapsulated Solar Cells for Passive Thermal Control', *IEEE J. Photovoltaics*, vol. 14, no. 3, pp. 459–465, May 2024, doi: 10.1109/JPHOTOV.2024.3372329.

[12] J. Zhou, Q. Yi, Y. Wang, and Z. Ye, 'Temperature distribution of photovoltaic module based on finite element simulation', *Solar Energy*, vol. 111, pp. 97–103, Jan. 2015, doi: 10.1016/j.solener.2014.10.040.

[13] B. Zhao, M. Hu, X. Ao, and G. Pei, 'Performance analysis of enhanced radiative cooling of solar cells based on a commercial silicon photovoltaic module', *Solar Energy*, vol. 176, pp. 248–255, Dec. 2018, doi: 10.1016/j.solener.2018.10.043.

[14] U. Banik *et al.*, 'Enhancing passive radiative cooling properties of flexible CIGS solar cells for space applications using single layer silicon oxycarbonitride films', *Solar Energy Materials and Solar Cells*, vol. 209, p. 110456, Jun. 2020, doi: 10.1016/j.solmat.2020.110456.

[15] K. Chen, K. Hu, B. Zhao, T. Chen, Y. Hao, and G. Pei, 'Spectral Selectivity of CdTe Cells with Substrate Configuration for Photovoltaic/Thermal Applications', *J. Therm. Sci.*, vol. 33, no. 4, pp. 1542–1553, Jul. 2024, doi: 10.1007/s11630-024-1979-z.

[16] M. Cagnoni, P. Testa, J. S. Dolado, and F. Cappelluti, ‘Extended detailed balance modeling toward solar cells with cement-based radiative coolers’, *Progress in Photovoltaics: Research and Applications*, vol. n/a, no. n/a, 2023, doi: 10.1002/pip.3758.
[17] S. V. Boriskina, ‘An ode to polyethylene’, *MRS Energy & Sustainability*, vol. 6, p. E14, Jan. 2019, doi: 10.1557/mre.2019.15.
[18] M. Yamaguchi *et al.*, ‘Analysis of temperature coefficients and their effect on efficiency of solar cell modules for photovoltaics-powered vehicles’, *J. Phys. D: Appl. Phys.*, vol. 54, no. 50, p. 504002, Dec. 2021, doi: 10.1088/1361-6463/ac1ef8.